Ionic Strength Dependence of Localized Contact Formation Between Membranes: Nonlinear Theory and Experiment

W. T. Coakley,* D. Gallez,# E. Ramos de Souza,#§ and H. Gauci*

*School of Biosciences, Cardiff University, Cardiff CF1 3TL, United Kingdom; #Service de Chimie Physique and Center for Nonlinear Phenomena and Complex Systems, CP 231, Universite Libre de Bruxelles, Campus Plaine, 1050 Brussels, Belgium; and §Instituto de Biofisica Carlos Chagas Filho, UFRJ, CCS, Cidade Universitaria, Ilha do Fundao, 21949-900 Rio de Janeiro, RJ Brazil

ABSTRACT Erythrocyte membrane surface or suspending phase properties can be experimentally modified to give either spatially periodic local contacts or continuous contact along the seams of interacting membranes. Here, for cells suspended in a solution of the uncharged polysaccharide dextran, the average lateral separation between localized contacts in spatially periodic seams at eight ionic strengths, decreasing from 0.15 to 0.065, increased from 0.65 to 3.4 μm. The interacting membranes and intermembrane aqueous layer were modeled as a fluid film, submitted to a disjoining pressure, responding to a displacement perturbation either through wave growth resulting in spatially periodic contacts or in perturbation decay, to give a plane continuous film. Measured changes of lateral contact separations with ionic strength change were quantitatively consistent with analytical predictions of linear theory for an instability mechanism dependent on the membrane bending modulus. Introduction of a nonlinear approach established the consequences of the changing interaction potential experienced by different parts of the membrane as the disturbance grew. Numerical solutions of the full nonlinear governing equations correctly identified the ionic strength at which the bifurcation from continuous seam to a stationary periodic contact pattern occurred and showed a decrease in lateral contact and wave crest separation with increasing ionic strength. The nonlinear approach has the potential to recognize the role of nonspecific interactions in initiating the localized approach of membranes, and then incorporate the contribution of specific molecular interactions, of too short a range to influence the beginning of perturbation growth. This new approach can be applied to other biological processes such as neural cell adhesion, phagocytosis, and the acrosome reaction.

INTRODUCTION

Erythrocyte membrane adhesion by lectins or macromolecules has been extensively studied as a model system in which to establish some general properties of membrane interaction (Fisher, 1993; Gallez and Coakley, 1996; Sung and Kabat, 1994). The erythrocyte model system has been used to discriminate between interaction conditions resulting in two distinctly different outcomes of adhesion, i.e., formation of a continuous contact seam or the making of arrays of discrete contacts, separated by distances of the order of a micron, along the seam (Thomas and Coakley, 1995). Modifications of membrane interaction that increase net attraction (e.g., enzymatic depletion of glycocalyx charge and/or mass; increased macromolecular concentration or mass) can bring about an outcome transition from a uniform contact seam to one characterized by localized discrete contacts (Gallez and Coakley, 1996). It has been shown that the greater the increase in net attraction the shorter the separation distance, in the lateral direction, between contact points (Thomas and Coakley, 1995). Local contact formation is also observed when erythrocyte adhesion is induced by some lectins (Darmani and Coakley, 1991).

The observation of two possible (continuous or punctuated) forms of contact seam in the experimental model system has been interpreted from the perspective of interfacial instability theory (Gallez and Coakley, 1996). This approach treats two interacting membranes and the intermembrane water layer as a thin fluid film separated from the cytoplasms of the interacting cells by transition zones, modeled as two-dimensional surface phases with appropriate physical chemical properties such as bending modulus, surface tension, and surface charge (Dimitrov and Jain, 1984; Gallez and Coakley, 1986, 1996). The deformation of a plane interface arising from a small perturbation can be expressed as a Fourier integral so that it suffices to determine the response of the system to simple sine or cosine disturbances. The system is unstable if a sine or cosine disturbance of any wavelength may grow. The wavelength with the fastest growth rate will dominate systems that are unstable over a range of wavelengths. The formation of spatially periodic contacts between interacting membranes is treated here as an example of a squeezing (SQ) mode instability, i.e., a situation where the central plane of an initially plane film remains flat but spatially periodic variations in film thickness develop and grow, leading to rupture or to pattern formation in the contact zone.

An experimental model system has been developed here in which pronase pretreatment of erythrocytes reduces glycocalyx stereorepulsion, at the same time removing some cell surface charge but retaining sufficient charge to exert a significant electrostatic repulsion (Baker et al., 1993; Thomas and Coakley, 1995). The cells are incubated with

Received for publication 10 June 1998 and in final form 27 April 1999.

Address reprint requests to Prof. W. T. Coakley, School of Biosciences, Cardiff University, Cardiff CF1 3TL, UK. Tel.: 44-1-222-874287; Fax: 44-1-222-874305; E-mail: sabwtc@cardiff.ac.uk.

0006-3495/99/08/817/12 $2.00

the uncharged polysaccharide, dextran, so that polymeric cross-bridging and depletion forces appear in the intercellular gap. When the ionic strength of the suspending phase of such cells is altered the electrical forces change while the nonelectrical forces remain unaffected. Ionic strength is therefore an appropriate control parameter with which to explore interaction mechanisms. An earlier study (Thomas and Coakley, 1995) showed, in agreement with linear interfacial instability theory, that the lateral separation of contact points between cells in dextran increased with decrease in the ionic strength of the suspending phase. Results were limited to three ionic strengths. When experimental variances in results at each ionic strength were considered, it was not possible to go the further step and differentiate between bending and tension control of mechanism. In the present study the number of ionic strengths at which data have been obtained has been increased. Attention has been directed to the distribution of wavelengths at each ionic strength so that characteristic wavelengths can be more precisely identified. It is argued that the new extended data are consistent with a bending-controlled interfacial instability.

Experimental data have previously been considered solely from a linear stability analysis. A recently developed nonlinear approach (De Wit et al., 1994; Gallez et al., 1996; Ramos de Souza and Gallez, 1998) is applied now to extend insight beyond the linear theory results that gave conditions for which a disturbance can begin to grow. In this paper we follow the evolution of that growth as different parts of the membrane experience different disjoining pressures. The emergence of patterns of spatially periodic close approach of membrane and the dependence of the minimum distance of approach on ionic strength are shown. The ionic strength dependence of the lateral separation between locations of close approach is in agreement with experiment. A bifurcation in membrane displacement with ionic strength, identified by the numerical simulations of the nonlinear approach, is in agreement with the experimentally observed transition from parallel contact topology to localized discrete contacts.

The different biophysical micromechanical adhesive properties of continuous and focal contact seams have already been distinguished by Ward and Hammer (1993). Conditions under which membrane interaction can spontaneously result in localized membrane contacts, as demonstrated here, may also be of general biological interest because local contacts are a feature of such processes as cellular migration and differentiation (Burridge and Chrzanowska-Wodnicka, 1996), neural cell adhesion (Rutishauser and Landmesser, 1996), phagocytosis, and the acrosome reaction (Bawa et al., 1993). Extension of the present work to specific adhesion with receptor-ligand binding will be briefly discussed.

MATERIALS AND METHODS

Experimental

The preparation of the cell samples has previously been described (Thomas and Coakley, 1995). Essentially, human erythrocytes were drawn by finger prick, washed, resuspended in 145 mM saline with 5 mM phosphate buffer (PBS) at pH 7.32, and exposed to 0.5 mg ml^{-1} pronase (Boehringer Mannheim, Lewes, Sussex, U.K.) for 20 min.

The zeta potential of cells in a washed aliquot of these enzyme-treated erythrocytes was determined in a cell cytophorimeter (Zetamaster, Malvern Insts., Ltd., Malvern, U.K.) as being 8 mV.

The main cell volume was washed and resuspended in buffered saline of different NaCl concentrations where cell volume was maintained through pH adjustment (Hoffman and Laris, 1974) and osmolality was maintained at 278 mOsm by addition of sorbitol. Cells were then exposed to 6% w/v concentration of 72 kDa dextran in the different ionic strength saline solutions for 30 min with occasional shaking. The cells were then fixed with glutaraldehyde to give a final fixative concentration of 3%, and examined by 63× oil immersion microscopy or by transmission electron microscopy.

Cells (both single cells and cells in dextran-induced clumps) in a number of light microscopy fields of view, to a total of ~200 cells, were examined at each ionic strength. The percentage of adhered cells in a sample was estimated from those of the 200 cells that were in clumps. The form of the contact between adhered cells, whether continuous parallel or spatially periodic, was also scored during light microscopy, and the percentage of cells with continuous parallel seams was calculated.

The average lateral separation distance between contact points along spatially periodic seams was calculated from transmission electron micrographs. The number of contact seams scored at each ionic strength ranged from 26 to 81, with an average of 53. Cumulative frequency distributions of the average lateral separation were calculated.

Theoretical model

The interaction zone between two cells will be modeled as a free film with tangentially immobile surfaces. The following hypotheses are considered, in the context of adhesion of red blood cells.

First, we do not consider diffusion of surface molecules, since (1) the spectrin-based membrane skeleton of erythrocytes significantly constrains lateral diffusion of its anion channels and potentially limits the mobility of proteins, such as charge-bearing glycophorin A, that can complex with the anion exchanger (Bennett and Gilligan, 1993); and (2) Darmani et al. (1990) found, by ferrinin-labeled antibodies and freeze-fracture electron microscopy, no local accumulation of the charge-carrying glycophorins on the surfaces of erythrocytes forming spatially periodic contact during agglutination by the sialic acid "specific" lectin, wheat germ agglutinin. The role of lateral motion of molecules on cell adhesion in general will be discussed at the end of the paper.

Second, the two surfaces of the film are considered as symmetric about the plane that bisects the contact zone normal to the line segment connecting the cell centers. This hypothesis is justified by the fact that the population of the cells is relatively homogeneous and that the observed periodic patterns show this symmetry. In terms of the model, this corresponds to the prediction of an unstable squeezing mode (SQ) with the two surface 180° out of phase, decoupled from the bending mode (where only in-phase deformation of the two surfaces occur).

Third, the interaction forces are nonspecific forces (electrical, van der Waals, steric, cross-bridging, and/or depletion forces). The interaction potentials are balanced at a secondary minimum in a region where the change of electrical forces with ionic strength is significant. The primary minimum occurs at very short separation distances (on the scale of the range of receptor-ligand bonds. The latter are not considered here).

The mean film thickness, h_0, is defined as the distance between the outer edges of the glycocalyxes of the two cells. The equation for the evolving film thickness $h(x, t)$, in the long wavelength approximation is given (Prevost and Gallez, 1986) in dimensionless form by

$$h_t = -(1/4)[\phi_x h^3 + \sigma_T h_{xxx} h^3 - B h_{xxxxx} h^3]_x \qquad (1)$$

where σ_T is the total surface tension (membrane tension of both cells plus repulsive and attractive contributions to film tension), B is the bending

modulus of the membranes, and ϕ is the total disjoining pressure, i.e., the difference between the pressures in the film and bulk phases. This disjoining pressure is characterized as the sum of its electrostatic ϕ_E and nonelectrostatic ϕ_N parts:

$$\phi = \phi_E + \phi_N \tag{2}$$

The electrostatic part ϕ_E makes a repulsive contribution, since both surfaces are negatively charged, that is given (Hiemenz, 1986) for low electric surface potential ψ_0 by

$$\phi_E = (16 n_0 (e\psi_0)^2/kT) \cdot \exp(-\kappa h) = P_E \exp(-\kappa h) \tag{3}$$

where n_0 is the concentration of counterions, ψ_0 is the surface potential, k is Boltzmann's constant, T is the absolute temperature, and e is the electronic charge. κ, the inverse of the Debye length, is given by

$$\kappa = (8\pi e^2 n_0/kT)^{1/2} \tag{4}$$

Both P_E and κ can therefore be calculated from the experimental parameters. It has been argued that the fall of surface potential with distance from the bilayer is small through the volume-charged bulk of the glycocalyx (Donath and Voigt, 1983) and that the potential at the edge of the glycocalyx is smaller than that estimated classically from zeta potential measurements (Levine et al., 1983). Within the limitations of present models of the glycocalyx and its charge distribution, the cell surface potential (ψ_0), localized at the edge of the glycocalyx 5 nm from the bilayer (Viitala and Jarnefelt, 1985), will be taken as 4 mV (half of the measured zeta potential).

To a first approximation also, ϕ_N includes the disjoining pressure from van der Waals attractive forces, stereorepulsive forces associated with the glycocalyx (Foa et al., 1996), and forces due to the dextran polymers. These interactions together make a net attractive contribution that is independent of change in the ionic strength. There is ample experimental evidence showing that adhesion molecules like dextran are necessary to bring together lipid bilayers and cells against repulsive electrostatic force (Evans, 1995). A problem, at the present time, is that of distinguishing between the relative contributions of macromolecular cross-bridging (Snowden et al., 1991) of cells by dextran reversibly adsorbing to the erythrocyte glycocalyx (Chien et al., 1977; Jan, 1979) and the attractive effects of a (partially) depleted molecular layer of dextran (Donath et al., 1989) at the glycocalyx surface. Adhesion of red blood cells is characterized by lower adhesion energies than is the case for smooth lipid bilayers. This difference is probably due to the penetration of dextran molecules in the complex glycocalyx structure (this point will be discussed in more detail in the Results section). The repulsion due to steric hindrance of the glycocalyxes will be included here through this reduction between attractive forces. In addition, at the secondary minimum, the van der Waals forces are negligible compared to depletion forces (Evans, 1989).

We begin with the simplistic assumption that the net attractive effect in the region between the outer parts of the glycocalyxes (where the electrostatic interactions are operative) has the following exponential form:

$$\phi_N = -P_N \exp(-\kappa_N h) \tag{5}$$

where P_N and κ_N are the amplitude and inverse of the characteristic length of the net nonelectrostatic forces. Those parameters are estimated below for our experiments. We draw some general conclusions from the resulting numerical simulations. We then attribute the dominant attraction to depletion forces alone, where the form of an interaction potential profile, consisting of an attraction that has an initial essentially constant region followed by an exponential decrease with increasing membrane separation, has been established for liposome adhesion by dextran (Evans and Needham, 1988; Evans, 1989). We show that the features of disturbance growth emerging from the numerical simulation employing a simple exponential profile for the nonelectrical component of the disjoining pressure are preserved when the profile is given the form determined experimentally for liposome interactions in dextran (Evans and Needham, 1988).

Linear analysis

In order to understand the onset of the deformation of the interfaces of the film, it is sufficient to characterize the spatiotemporal evolution of small disturbances around the steady-state solution of the nonlinear equation. The equation for the film thickness $h(x, t)$ (Eq. 1) can be linearized around the plane steady-state solution of thickness h_0, which corresponds to the average thickness of the film. In dimensionless form, this steady-state solution is $h_0 = 1$. We take normalized $h = 1 + 2H$, where H is a small perturbation at each interface, and obtain the linearized equation (with the term $d\phi/dh$ evaluated at $h = 1$)

$$H_t = -1/4[\sigma_T H_{4x} - B H_{6x} + d\phi_{lin}/dh\, H_{2x}] \tag{6a}$$

with

$$d\phi_{lin}/dh = [d\phi/dh]_{h=1} = -\kappa P_E \exp(-\kappa) + \kappa_N P_N \exp(-\kappa_N) \tag{6b}$$

Solutions of the form $\Delta \cdot \exp(iqx + \omega t)$, where Δ is a small amplitude parameter, give the characteristic equation:

$$\omega = -q^2/4[\sigma_T q^2 + B q^4 - d\phi_{lin}/dh] \tag{7}$$

This provides a relation for the dominant wavelength, i.e., the wavelength $\lambda_m = 2\pi/q_m$, at which the rate of growth is maximum ($d\omega/dq = 0$):

$$\lambda_m \approx 2\pi[\sigma_T/d\phi_{lin}/dh]^{1/2} \qquad \text{if the bending is negligible} \tag{8a}$$

$$\lambda_m \approx 2\pi[B/d\phi_{lin}/dh]^{1/4} \qquad \text{if the tension is negligible} \tag{8b}$$

Note that the value $d\phi_{lin}/dh$ must be positive to have an instability (attractive nonelectrical forces higher than repulsive electrical forces, see Eq. 6b). The derivative of the disjoining pressure may also be expressed as the curvature (second derivative with respect to separation distance in the normal direction) of the membrane interaction potential V, since $\phi = -dV/dh$. It follows from Eq. 8 that, where it is possible to quantify $d\phi/dh$ at the onset of growth of the dominant instability, a log-log plot of λ against $d\phi/dh$ should have a slope of -0.5 or -0.25 where, respectively, membrane stretching or membrane bending determines the outcome of the membrane interaction.

Numerical simulations

The dimensionless full nonlinear Eq. 1 is solved numerically using a FTCS (forward time centered space) schema (Press et al., 1989). The physical idea is to introduce a small perturbation on a flat homogeneous film of thickness h_0 (dimensionless, = 1) and follow the evolution of this perturbation for finite size deformation. The perturbation is expressed by a (random or periodic) initial condition $h(x, 0)$ at $t = 0$. Periodic boundary conditions are applied at the film borders, so that the system will be described as an infinite nonbounded film. Comparison with a simulation for fixed boundary conditions will also be performed. The dimensionless values of the parameters in Eq. 1 are calculated from the respective dimensional values (barred) for red blood cells in physiological solutions: $\bar{\rho} = 1$ g/cm^3; $\bar{\nu} = 0.01$ cm^2/s; $\bar{h}_0 = 12$ nm; $\bar{\sigma}_T = 0.1$ dyn/cm (see McIver and Church, 1982); $\bar{B} = 1.8\ 10^{-12}$ dyn $\cdot$ cm (Evans, 1983).

Here, $\bar{\rho}$ is the density and $\bar{\nu}$ is the kinematic viscosity of the thin aqueous film. The expressions for P_E and κ^{-1} (Eqs. 3 and 4) contain terms in counterion concentration. Values of κ^{-1} range from 1.195 nm to 0.787 nm, respectively, for buffered 60 mM and 145 mM NaCl. However, substituting in Eq. 3 for the corresponding values of the surface potential shows that the values of P_E are essentially constant ($\bar{P}_E = 1.4 \times 10^6$ dyn/cm^2) for the different ionic strengths, since change of counterion concentration n_0 causes a compensating change in surface potential.

We consider that the dominant wavelength obtained from the linear analysis is of the order of the distance between the contact points measured

in the experiment ($\bar{\lambda}_m \sim 1$ μm). Taking into account both bending and tension, the dimensional value of λ_m can be determined from Eq. 7, taking $d\omega/dq = 0$, as

$$\bar{\lambda}_m = 2\pi[(1/3\bar{B}(-\bar{\sigma}_T \pm (\bar{\sigma}_T{}^2 + 3\bar{B}\, d\bar{\phi}_{lin}/dh)^{1/2})^{1/2}]^{-1} \quad (9a)$$

with

$$d\bar{\phi}_{lin}/dh = -\bar{\kappa}\bar{P}_E\exp(-\bar{\kappa}\bar{h}_0) + \bar{\kappa}_N\bar{P}_N\exp(-\bar{\kappa}_N\bar{h}_0) \quad (9b)$$

Substituting for the known quantities on the right-hand side of Eq. 9a and setting $\bar{\lambda}_m = 1$ μm results in an estimate of $d\phi_{lin}/dh$. We then choose values of $\bar{\kappa}_N{}^{-1}$ in the range 3–5 nm to take into account the fact that, for adhesion to occur, the range of nonelectrical forces is likely to be longer than the range of the electrostatic repulsion (which is $\approx$1 nm). Then substituting, for example, 5 nm for $\kappa_N{}^{-1}$ in Eq. 9b leads to a value of $\bar{P}_N \approx 1.2 \times 10^5$ dyn/cm^2. These values of $\bar{\kappa}_N{}^{-1}$ and $\bar{P}_N$ are also plausible, since they fall within the ranges 1.6 nm to 5 nm and 10^4 dyn/cm^2 to 10^6 dyn/cm^2, respectively, determined from measurement and surface depletion theory for dextran adhesion of liposomes (Evans and Needham, 1988).

The dimensionless values used in the numerical simulations are related to their dimensional counterparts by

$$\sigma_T = \bar{h}_0\bar{\sigma}_T/\bar{\rho}\bar{\nu}^2 \quad B = \bar{B}/\bar{h}_0\bar{\rho}\bar{\nu}^2 \quad (10)$$

$$P_E = \bar{h}_0{}^2\bar{P}_E/\bar{\rho}\bar{\nu}^2 \quad 1/\kappa = 1/\bar{\kappa}\bar{h}_0$$

$$P_N = \bar{h}_0{}^2\bar{P}_N/\bar{\rho}\bar{\nu}^2 \quad 1/\kappa_N = 1/\bar{\kappa}_N\bar{h}_0$$

The same average distance $\bar{h}_0$ is used to adimensionalize all the parameters for the different values of the ionic strength (see Discussion). The dimensionless length L of the contact zone is taken to be of the order of 150, so that the corresponding dimensional length will be of the order of 150×12 nm = 1.8 μm, which represents a reasonable fraction of the contact zone. As periodic boundary conditions are applied, this will be sufficient to describe the patterns (they will be repeated along the interaction seam because of the periodic boundary conditions).

RESULTS

Cell adhesion and contact seam morphology

Light microscopy showed that the percentage of cells with wavy profiles increased and, consequently, that for parallel contact decreased (Fig. 1) with increasing ionic strength. The triplicated experiments show consistency among batches of cells from blood drawn and processed on different days.

The electron micrographs of Fig. 2 show an example of parallel contact in low ionic strength medium (65 mM NaCl) together with representative examples of the decreasing lateral separation of contact sites in suspending phases of higher ionic strength. A threshold for appearance of local contacts is thus identified experimentally as being $\sim$70 mM NaCl. The decrease in average lateral separation (determined from transmission electron micrograph measurements) of contacts in seams with wavy profile is shown for increasing ionic strengths in Fig. 3. The percentage of cells involved in adhesion is also shown in Fig. 3. The slope of the best fit straight line to the adhesion data was not significantly different from zero ($p = 0.28$). It follows that, while the contact topology was ionic strength-dependent, the percentage of cells involved in contact formation was not.

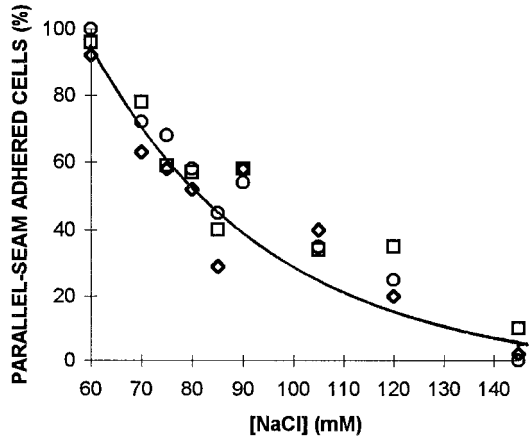

FIGURE 1 The percentage of membrane-membrane contact seams that had a continuous parallel-membrane topology when formed in different concentrations of NaCl. The symbols represent data from three different experiments.

Cumulative frequency distributions of average lateral contact separation per seam at the different ionic strengths are shown in Fig. 4. The results imply that, for a given ionic strength, the innate cell surface properties (i.e., a combination of elastic constants, glycocalyx charge, and structure) determining lateral separation of contacts were not the same for each cell, i.e., the properties have a distribution across the population. Since the percentage of adhered cells showing continuous parallel contacts decreases with increase in ionic strength (Fig. 1), it follows that the range of innate surface properties of the fraction of the cell population contributing to the average lateral separation (Fig. 3) was different at the different ionic strengths. Consequently, the association of a measure of lateral separation with ionic

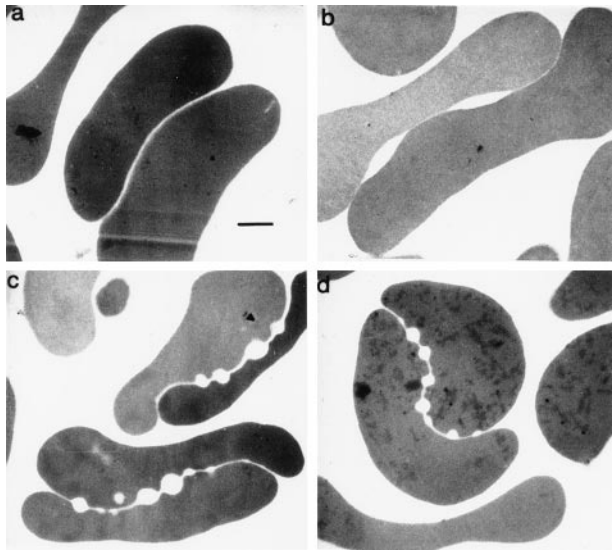

FIGURE 2 Electron micrographs of contact seams showing (*a*) a continuous seam of contact in 65 mM NaCl and examples of (*b*) long, (*c*) medium, and (*d*) short lateral contact separation distances in 80, 105, and 145 mM NaCl, respectively. The bar represents 1.0 μm for the four cases.

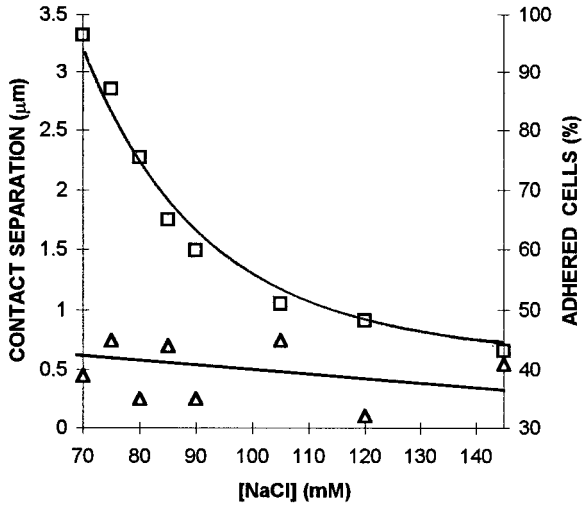

FIGURE 3 The average lateral distance between localized membrane-membrane contacts (□) and the percentage of suspended cells that adhered (△) in different concentrations of NaCl.

strength must be refined beyond the use of an arithmetic sample mean when considering the dependence of change in lateral contact separation on change in ionic strength.

Relationship of experimental wavelength and disjoining pressure: linear theory

The cumulative frequency data (Fig. 4) were considered with the data of Fig. 1 in order to associate a specific wavelength with a change in ionic strength, as shown in the following example. Fig. 1 shows that 23 and 35% of seams had continuous parallel topology at NaCl concentrations of 120 and 105 mM, respectively. Consequently, the percentage of wavy seams at these ionic strengths were 77 and 65%

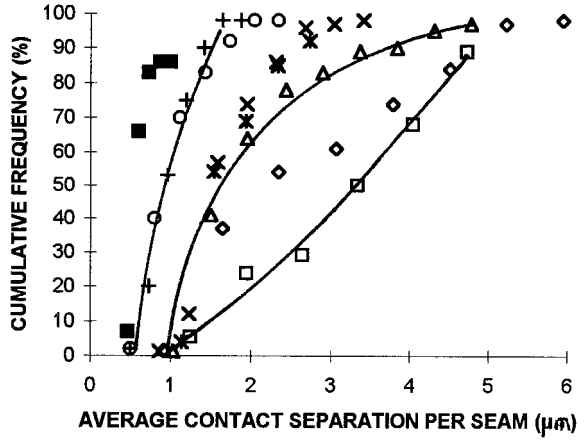

FIGURE 4 Cumulative frequency distributions of the average lateral contact separation per seam for cells adhered in 145 (■), 120 (+), 105 (○), 90 (*), 85 (×), 80 (△), 75 (◇), and 70 (□) mM NaCl. The representative trends (left to right) are for 120, 80, and 70 mM [NaCl]. The number of contact seams for which average separations were calculated at [NaCl] ranged from 26 to 81, with an average of 53.

of the total number of seams, respectively. It follows that only (65/77) × 100, i.e., 84% of the seams that had localized contacts at 120 mM NaCl, also made such contacts at 105 mM NaCl. The wavelength corresponding to 84% of the 120 mM NaCl distribution was read from Fig. 4. This wavelength was taken as that which could be suppressed by a [NaCl] change from 120 to 105 mM. Since only the electrical part of ϕ (Eq. 2) changes with ionic strength, the change in the gradient of the disjoining pressure may be derived from the electrostatic component ϕ_E (Eq. 3) alone. Values of $\Delta(d\phi_E/dh)$ were calculated, over a range of values of h, for NaCl concentration change from 120 to 105 mM. A second wavelength and related set of $\Delta(d\phi_E/dh)$ for different values of h was obtained for the NaCl concentration change from 120 to 90 mM. In this way sets of wavelength data and corresponding $\Delta(d\phi_E/dh)$ values were obtained for each ionic transition, "starting" from 120, to 105, 90, 85, 80, 75, and 70 mM NaCl; "starting" at 105 to 90, 85, 80, 75, and 70 mM, and so on.

The resulting λ, $\Delta(d\phi_E/dh)$ data were plotted for fixed values of h in the range 5–14 nm, as log-log plots in order to search for a power law relationship between the λ and $\Delta(d\phi_E/dh)$ data (Eq. 8). It was found that, for a fixed h, the slopes of the data subsets obtained from the different "starting" ionic strengths were broadly similar, but that the "intercept" value for the straight line equation of the different log-log transformed data subsets increased significantly as the "starting" ionic strength of the subset was decreased. Since the intercepts should reflect a physical membrane constant (B or σ_T (Eq. 8)), such an outcome was not acceptable and the implied assumption that the value of h at which the system became unstable (h_{init}) was the same for all ionic strengths was modified. Consequently, the subsets of data for each "starting" [NaCl] were confined to not more than three points, relating to those ionic strengths nearest to that of the "starter," in order to reduce inaccuracy arising from large [NaCl] increments. We note here that when h_{init} was taken as 5 nm and, for consistency of later comparison, the three points per subset limit was applied, the gradients were −0.24, −0.29, −0.27, and −0.28 for "starter" NaCl concentrations of 120, 105, 90, and 85 mM, respectively. These slopes were consistent with a bending modulus rather than a tension-controlled mechanism (Eq. 8). Increased h_{init} resulted in some decrease rather than increase in gradient, again leading away from a tension-controlled mechanism. A plot of $\log(\lambda)$ against $\log(\Delta(d\phi_E/dh))$ gave values of the bending modulus close to the published values of 2×10^{-12} dyn·cm. The 95% confidence limits for the slope in Fig. 5 are -0.267 ± 0.031. The sets of data in Fig. 5 were for suppression of waves in 1) 120 mM by reducing to 105, 90, 85 mM; 2) 105 mM by reducing to 90, 85, 80; 3) 90 mM by reducing to 85, 80, 75; 4) 85 mM by reducing to 80, 75, and 70 mM; 5) 80 by reducing to 75 and 70 mM. Taking a slope of −0.25 and setting a line to pass through the mean values of $\log(\lambda)$ and $\log(\Delta(d\phi_E/dh))$ gives, from Eq. 8a, a B value of 4×10^{-11} dyn·cm.

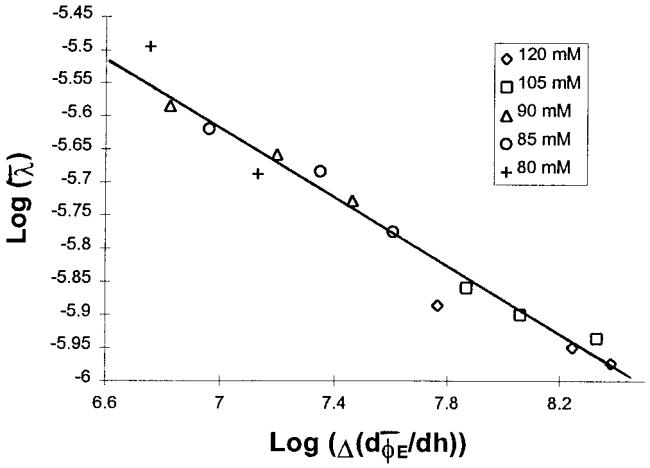

FIGURE 5 The dependence of the lateral separation distance of local contacts (deduced from data on topology of contact formation (Fig. 2) and cumulative frequency distributions of NaCl concentrations of lateral separations (Fig. 4)) on related change in the gradient of the electrostatic disjoining pressure for different reference [NaCl]. The sets of data are for suppression of waves in reference [NaCl] of 1) 120 mM by reducing to 105, 90, 85 mM; 2) 105 mM by reducing to 90, 85, 80; 3) 90 mM by reducing to 85, 80, 75; 4) 85 mM by reducing to 80, 75, and 70 mM; 5) 80 mM by reducing to 75 and 70 mM. The normal-direction membrane separation distance (h_{init}), at which the aqueous film became unstable, was taken as 9.5, 10, 12, 12, and 13 nm for the decreasing reference [NaCl] respectively.

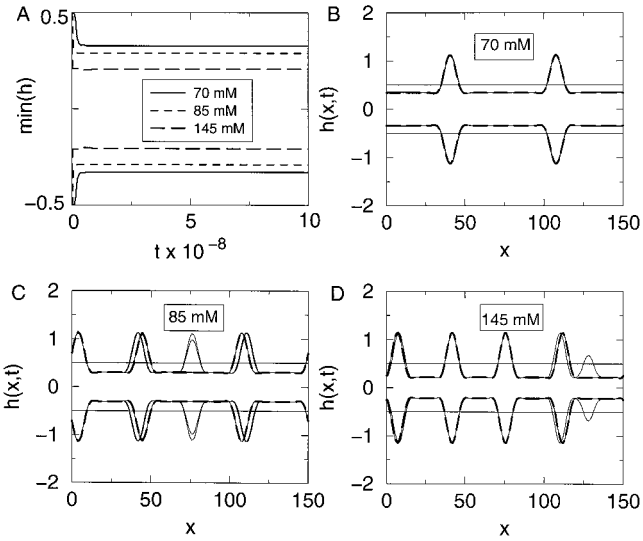

FIGURE 6 The formation of [NaCl]-dependent stable patterns at 70, 85, and 145 mM. The dimensional parameter values of the system are: $\bar{\sigma}_T = 0$; $\bar{B} = 1.8 \times 10^{-12}$ dyn·cm; $\bar{P}_E = 1.4 \times 10^6$ dyn/cm^2; $\bar{P}_N = 1.2 \times 10^5$ dyn/cm^2; $1/\bar{\kappa}_N = 5.0 \times 10^{-7}$ cm; $1/\bar{\kappa} = 1.113 \times 10^{-7}$, 1.016×10^{-7}, and 0.787×10^7 cm for 70, 85, and 145 mM [NaCl], respectively. The film is perturbed at $t_0 = 0$. Random initial condition (RIC) and periodic boundary conditions (PBC) are adopted. Both upper and lower surfaces are shown. (*a*) Min(h) as function of dimensionless time. Min(h) decreases as [NaCl] increases. The stable patterns are reached at dimensionless time $t_f = 10^9$ (dimensional time of the order of 0.1 s); *B–D* show the spatiotemporal curves $h(x, t)$ at time steps of $t_f/10$. The stable patterns $h(x, t_f)$ are represented by the long-dashed lines. The greater the salt concentration the smaller the lateral distance between contact points. The (mean) dimensional values of the lateral distance between contact points are ~0.9, ~0.6, and ~0.45 μm, respectively.

Nonlinear simulations

Role of the ionic strength

We consider several simulations where [NaCl] is increasing from 60 mM to 70, 85, and 145 mM. The purpose of these simulations is initially to check the presence of a threshold for the transition from plane parallel to periodic patterns of contact points and then to try to reproduce and control the variation, with ionic strength, in wavelength of the periodic patterns.

The results of the first set of simulations are shown on Fig. 6. Periodic boundary conditions are used, while initial conditions are at random. The dimensional parameters values are membrane bending modulus $\bar{B} = 1.8 \times 10^{-12}$ dyn·cm, electrical parameter $\bar{P}_E = 1.4 \times 10^6$ dyn/cm^2, the Debye length decreases from 1.113 nm to 1.016 and 0.787 nm for 70, 85, and 145 mM [NaCl], respectively. We first tested the role of the membrane bending, independently of the tension, so that the membrane tension $\bar{\sigma}_T = 0$. The nonelectrical parameters, $\bar{P}_N = 1.2 \times 10^5$ dyn/cm^2 and $\bar{\kappa}_N^{-1} = 5$ nm, are deduced as explained in Material and Methods. They will be the same for all the simulations, since the ionic strength has no influence of the nonelectrostatic parameters. The corresponding dimensionless parameter values used in the simulation are $\sigma_T = 0$, $B = 0.015$, $P_E = 0.02$, $\kappa^{-1} = 0.092$–0.065, $P_N = 0.0017$, and $\kappa_N^{-1} = 0.42$. For 60 mM NaCl (below the threshold), we first checked that for a small random perturbation, the system goes back to the homogeneous flat state (simulation not shown). The system is thus stable with respect to small perturbations (the real roots of the characteristic Eq. 7 are negative), and the surfaces of the approaching cells remain flat (see the experimental continuous seam shown in Fig. 2 *a*).

Fig. 6 illustrates situations where the system is unstable with respect to small perturbations and evolves subsequently to the formation of stable patterns. Both upper $h(x, t)/2$ and lower $-h(x, t)/2$ surfaces of the film are represented in order to describe the surfaces of the two approaching cells. Fig. 6 *A* shows that after a short time, small perturbations will increase (positive real values of the roots of the characteristic Eq. 7), and the minimum thickness evolves to a new stationary value, which represents the nodes of the squeezing (SQ) mode. This phenomenon was predicted in a bifurcation analysis for thin liquid films where attractive and repulsive forces are present (Erneux and Gallez, 1997). Further analytical developments and numerical simulations have been performed and compared to experiments on thin liquid films with insoluble surfactants (Ramos de Souza and Gallez, 1998). It can be seen in Fig. 6, *B–D* that the SQ mode describes a stationary symmetrical deformation at a final time, defined as t_f. Fig. 6 *A* shows that the minimum distance between the two cells decreases as the salt concentration increases. This is due to

the fact that the Debye length decreases with increasing salt concentration and the repulsion due to the overlap of the electrical double layers decreases (the same conclusion is expected from a standard DLVO theory for two flat interacting surfaces). The stable patterns are reached after a dimensional time of 0.1 s (using a viscosity of water value of the order of 10^{-2} poise). If we take into account the fact that some molecules of the glycocalyx may still protrude into the intercellular aqueous layer, the viscosity may be one order of magnitude higher, leading to a time for the formation of the patterns of the order of 1 s, which is in good agreement with experiments (Darmani and Coakley, 1990). Fig. 6, *B–D* show the spatiotemporal evolution of the two surfaces at different salt concentrations. It is clear that the wavelength of the pattern decreases with increasing salt concentration. The number of crests changes from two to three and four, respectively. The dimensional values of the lateral distance between the contact points is 0.9, 0.6, and 0.45 μm, respectively, for 70, 85, and 145 mM [NaCl].

Multiplicity of steady-state solutions

In Fig. 6, a selection of wavelengths is observed as time evolves. Indeed, the system will first select the wavenumber $q_n = n\pi/L$, which is nearest to the most probable (dominant) wavenumber given by the linear theory $q_m = 2\pi/\lambda_m$. After a lapse of time, a selection of wavelengths will occur toward longer wavelengths, but the time needed to switch to successive wavelengths becomes increasingly long. For the same set of parameters as Fig. 6 *B* (70 mM NaCl), Fig. 7 shows that the random perturbation evolves to various metastable patterns: the first (five-crest) metastable pattern appeared at $\sim t = 3 \times 10^7$, while at $t = 6 \times 10^7$, the pattern has three crests. A two-crested pattern finally arises at $\sim t = 10^8$ and does not change up to the end of the simulation for time $t_f = 10^9$. This phenomenon of metastability (Mitlin, 1993; Khanna and Sharma, 1997; Ramos de Souza and Gallez, 1998) is expressed as a multiplicity of steady-state solutions of Eq. 1 and appears in the numerical simulations of the nonlinear evolution equation. It comes from the fact that nonlinear equations follow the fluctuations for a long time, not only at the onset of the perturbation. It is important to realize that the nonlinear mode selection is much less sensitive to the wavenumber than the predictions of the linear theory for the dominant mode. In order to make reasonable predictions, we always take the steady-state solution at long time (here dimensionless 10^9) and perform the comparison between different simulations for the same dimensionless time.

Role of bending and tension

Let us consider now the respective role of the bending B and tension σ_T. Fig. 5 shows that the slope for the dependence of the lateral separation distance of local contacts on related changes in the gradient of the electrical disjoining pressure for different NaCl concentrations is close to -0.25. This

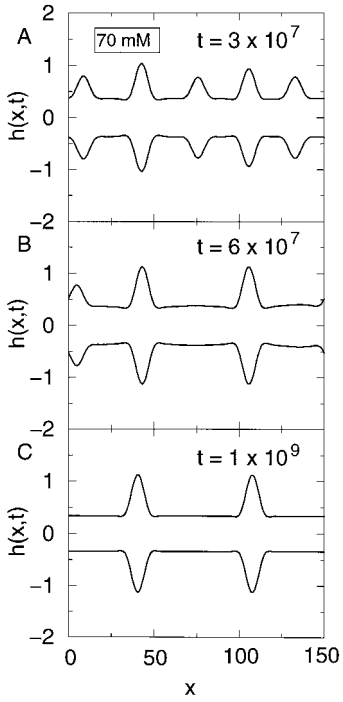

FIGURE 7 Multiplicity of stationary states. Spatiotemporal curves $h(x, t)$ at three different dimensionless times. The parameters have the same values as Fig. 6 *B* for 70 mM [NaCl]. Displayed patterns are metastable states with (*A*) five crests and (*B*) three crests that evolve to the final pattern (*C*) at $t_f = 10^9$.

is an indication of a bending mechanism controlling the instability.

The results for the simulations are shown in Fig. 8, *A* and *B* for two different values of the salt concentration. Periodic boundary conditions are also used, while initial conditions are at random. The dimensional parameters values B, P_E, P_N, and κ_N^{-1} are the same as in the previous figures, except that now we consider a surface tension σ_T of the order of 0.1 dyn/cm. For Fig. 8 *A,* [NaCl] is 70 mM (Debye length κ^{-1} of 1.113 nm), while for Fig. 8 *B,* [NaCl] is 145 mM (Debye length of 0.787 nm). We consider that the total surface tension σ_T is approximately constant as the ionic strength is changed (the electrostatic contribution to the total surface tension is small (Thomas and Coakley, 1995).

For the chosen values of bending and tension, Fig. 8 *A* shows that for [NaCl] of 70 mM, there is no difference between the two mechanisms, except for a sharper shape of the final pattern for the tension controlled system. The curve obtained for a bending controlled mechanism is similar to the curve obtained by combining a bending and a tension mechanism (we will call this a mixed mechanism) during the instability, as well as for the lateral distance between the contact points and for the normal distance between the contact points (crests). The curve for a tension mechanism agrees only for the distance between nodes, while the amplitude of the pattern is higher. However, as salt concentration is increased and the final patterns move to shorter wavelengths, the pattern itself will change. Fig. 8 *B* shows

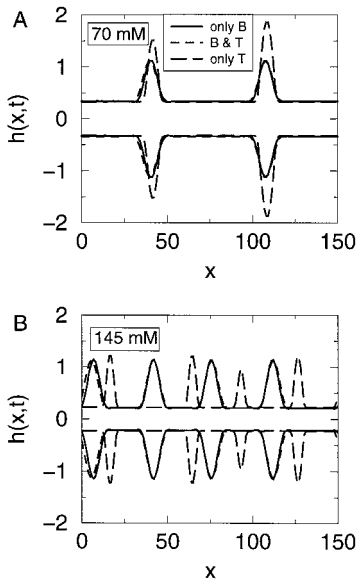

FIGURE 8 (*A*) The role of surface tension "T" and bending "B" at 70 mM [NaCl]. The dimensional values of the parameters are the same as in Fig. 6 *B,* with a surface tension $\bar{\sigma}_T = 0.1$ dyn/cm. Both RIC and PBC are adopted and the final state is shown. For the "only B" curve (*solid line*) $\sigma_T = 0$, whereas for the "only T" curve (*long-dashed line*) B = 0. The "only B" curve agrees with the "B & T" curve (*dashed line*) both for the distance between the contact points and for the distance between the crests. The "only T" curve agreed with the "B & T" curve for the distance between the contact points, but the amplitude of the pattern is larger. (*B*) The same as (*A*) but for 145 mM [NaCl]. The wavelength of the patterns decreases as the ionic strength increases in all cases. Again, the "only B" curve agreed with the "B & T" curve both for the distance between the contact points and for the distance between the crests. But in this case the "only T" curve has the same amplitude for the patterns and a nonregular period.

a similar amplitude for the tension-controlled system as for the bending or mixed system, but a nonregular period along the x axis: this can be interpreted as a tendency to switch to a shorter wavelength (the system always has to select integral values for the number of wavelengths).

It is difficult at the present time, because of the phenomenon of metastability discussed in the previous section, to verify precisely with the numerical simulations whether the wavelength dependence as a function of salt concentration is bending or tension-controlled. However, the comparison of Fig. 8, *A* and *B* already reveals that the bending mechanism (or the mixed mechanism) is consistent with the conclusions of Fig. 5, where a bending mechanism was suggested. The following qualitative argument can be developed: the linear stability analysis gives the variation of the dominant wavelength in the case of a bending mechanism (Eq. 8). At a certain value of h, the calculated value of $d\phi/dh$ will be the same for both mechanisms ($d\phi/dh$ is independent of B and σ_T), and could give the same wavelength for some particular values of the parameters B and σ_T, as in the numerical simulations of Fig. 8 *A*. As the ionic strength is increased, another calculated value of $d\phi/dh$ is obtained that is higher than the previous one, but again is the same for both mechanisms. However, due to the different power law (Eq. 8) the expected value of the dominant wavelength will be lower for the tension mechanism than for the bending mechanism, which is also predicted by the nonlinear approach (Fig. 8 *B*).

Role of initial conditions

Let us take now periodic initial conditions instead of random initial conditions. We will follow the evolution of the most probable wavelength, given by the linear analysis (Eq. 8b) in the case of a bending mechanism. The periodic initial condition is given by $h(x, 0)/2 = 0.5 + \Delta \cos(q_n x)$, with $q_n = n\pi/L$. The wavelength $\lambda_n = 2\pi/q_n$ is near the dominant wavelength.

For the same values of the parameters as in Fig. 6 *B* (70 mM [NaCl]), Fig. 9 *A* shows that the evolution to the final pattern is more rapid than for random initial conditions (since the most probable wavelength is already selected). Fig. 9 *B* shows that there is a small selection of wavelengths (from three to two) and the initial small periodic condition evolves naturally to a final periodic pattern of finite amplitude. The final wavelength and amplitude of the pattern are identical to those obtained for random initial conditions.

Role of depletion forces

Let us now discuss in more detail the role of a modification of depletion forces on the numerical results obtained so far, since the control of depletion forces with the polymer dextran is of interest in the interpretation of the experiments. To

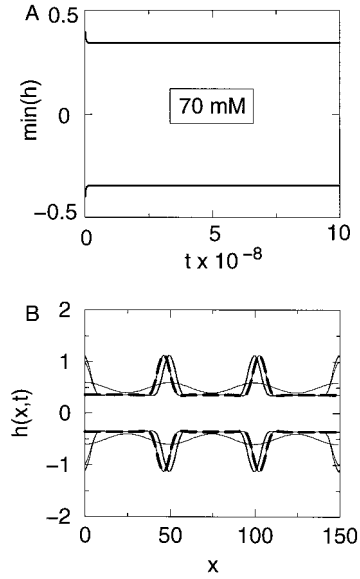

FIGURE 9 Role of initial conditions. The parameters are the same as in Fig. 6 *B*. Periodic initial conditions (PIC) of the form $h(x, 0)/2 = 0.5 + \Delta\cos(6\pi x/L)$ with dimensionless $\Delta = 10^{-1}$, instead of random initial conditions (RIC). (*A*) Min(h) as a function of dimensionless time; (*B*) spatiotemporal curves $h(x, t)$. The wavelength of the initial state (*solid line*) is that of the dominant wavelength of linear analysis, while the final wavelength (*long-dashed line*) is identical to that obtained with RIC.

achieve this goal, we will use here a more precise form of the nonelectrical disjoining pressure deduced from a theory of the nonspecific depletion molecular forces due to nonadsorbent macromolecules in solution (Evans and Needham, 1988; Evans, 1989). Because of its random movement, the polymer molecules will be moved away from the thin aqueous layer between the surfaces thus generating a reduction in the local osmotic pressure. The corresponding disjoining pressure has an exponentially decaying functional form whose amplitude is proportional to the polymer bulk concentration and whose decay length depends on both polymer concentration and polymer length. Experimental measurements of the disjoining pressure as a function of the distance between adherent lipid vesicles for three different molecular weight dextran molecules in two different concentrations (0.01 and 0.1 polymer volume concentration) have been reported (Evans, 1989). In our experiments, the concentration of 6% w/v corresponds to 0.0367 volume fraction, and the molecular weight is 72,000. However, we have to bear in mind the differences between lipid surfaces and cell surfaces. Considering that dextran is a random coil and will not easily penetrate the glycocalyx, we choose to keep the functional form of the depletion forces and introduce a cutoff distance. The nonelectrical disjoining pressure now reads:

$$\phi_N = -P_N \exp(-\kappa_N(h - d)) \qquad (11)$$

with P_N and κ_N^{-1} defined as previously and d a cutoff distance depending on the polymer. This cutoff distance increases as the molecular weight of the polymer increases (Evans, 1989). For the volume fraction and molecular weight of the experiments described here, we estimate a cutoff distance of the order of 3 nm.

Fig. 10 shows a nonlinear simulation performed for the same parameters as in Fig. 7, except for a cutoff distance $d = 3$ nm (in all the preceding simulations, $d = 0$ nm). The system first evolves to a metastable state with shorter wavelengths than in Fig. 7 (Fig. 10 *A*). The same selection of wavelengths appears then as time evolves (Fig. 10, *B* and *C*). The final pattern at $t_f = 10^9$ still shows a decrease in the wavelength and an increase in the amplitude of the pattern as compared to Fig. 7. From Eq. 11, it is clear that increasing the cutoff distance d will increase the attractive force between the cell surfaces. It has already been shown in other experiments that an increase in attractive forces always leads to a decrease in wavelengths (Gallez and Coakley, 1996).

Finally, it is interesting to test the role of fixed boundary conditions (FBC) and corresponding fluxes at the boundaries for the new functional form of the disjoining pressure given by Eq. 11. The numerical method was the same as for Fig. 10 except that the position of the two surfaces is fixed at the boundaries. The aqueous film has a finite length, and no periodicity is imposed. The expression of the boundary conditions does not imply conservation of mass inside the contact zone so that fluxes of water and/or nonadsorbing

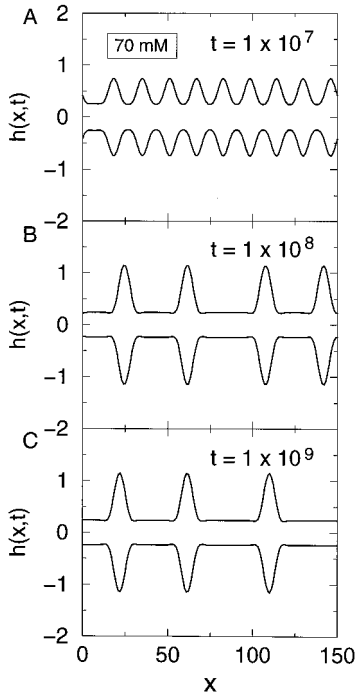

FIGURE 10 Role of depletion forces. Spatiotemporal curves at different dimensionless times, for the same values of parameters as Fig. 7 (70 mM [NaCl]), except that a cutoff distance $d = 3$ nm is introduced (Eq. 11). (*A* and *B*) A similar selection of wavelengths is observed, but the system evolves at final time ($t_f = 10^9$) toward a pattern with shorter wavelength and larger amplitude, due to the increase in attractive forces.

polymers are possible. This is particularly relevant in the presence of depletion forces. Preliminary results show the same selection of wavelengths as previously discussed, but the final pattern at dimensionless time 10^9 is only one-half wavelength (simulation not shown). This implies that there is a net flux of matter out of the interaction zone between the cells to the volumic phases. The type of boundary conditions considered (periodic or fixed) could thus affect the characteristics of the observed pattern, but the experimental system does not permit distinction between them at the present time.

DISCUSSION

The above work examines the conditions under which changes in nonspecific interactions, electrostatic in the present case, determine whether cell adhesion results in a parallel membrane contact seam of constant thickness or in a seam with a spatially periodic distribution of local contacts (Figs. 1 and 2).

It has long been known that electrostatic interaction can influence the extent of cell-cell adhesion, e.g., sialidase pretreatment of phagocytic monocytes (Weiss et al., 1966) or of their erythrocyte prey particles (Capo et al., 1981) increases phagocytosis. Phagocyte-prey attachment is also dependent on suspending phase ionic strength (Rabinovitch, 1971). The adhesion of erythrocytes on exposure to the

specific sialic acid binding lectin, wheat germ agglutinin, gives a contact seam of localized contacts at an average spacing of 0.65 μm (Darmani and Coakley, 1990). Current work here suggests that the spacing can be modulated by changes in ionic strength or by pronase depletion of the glycocalyx. The phagocytosis of glutaraldehyde-fixed horse red blood by *Acanthamoeba* involves interaction of an intrinsic amoeba lectin with mannose on the erythrocyte surface to form local contacts. The lateral separation of contacts increased from 0.65 to 1.6 μm on decreasing the ionic strength from 0.17 to 0.017 (Saghir, 1997).

The results discussed above suggest that nonspecific interactions can have a permissive role in allowing the specific ligand receptor interactions, known to be involved in many adhesion processes, to occur. It may also be noted here that the contribution of the physical properties (electrostatic, hydration (Yang et al., 1994), and steric (Rutishauser and Landmesser, 1996)) of neural cell polysialic acid molecules (PSA) in modulating neural cell adhesion receives continuing attention. The integral membrane glycoprotein neural cell adhesion molecule (NCAM) promotes cell-cell adhesion through a homophilic binding mechanism. Modulation of adhesion specifically arises from tightly controlled expression of different lengths (8–100 monomers (Rutishauser and Landmesser, 1996)) of the linear PSA that is attached to NCAM. Exposure of a richly PSA-expressing cultured F11 sensory neuron/neuroblastoma cell hybrid to a specific endoneuraminidase enhanced cell-cell aggregation by the L1 cell adhesion molecule, illustrating that regulation of the cell surface by PSA extends beyond binding by the NCAM polypeptide (Acheson et al., 1991). It has been observed that 1) while PSA is highly regulated in its expression its modulation of cell interactions probably arises from its unusual physical properties (Rutishauser, 1996) and 2) the role of PSA in neural structural plasticity may be paradigmatic for other large extensively hydrated highly charged surface carbohydrates such as glycosaminoglycan and proteoglycans (Flyer and Hockfield, 1996).

In the present work ionic strength change gives an essentially constant probability of cell adhesion by the relatively long-range attractive forces due to dextran, while at the same time resulting in a marked change in lateral contact region spacing (Fig. 3). The result is consistent with the distinction that interfacial instability theory makes between the influence of interaction potential on adhesion and the gradient of disjoining pressure (curvature of the interaction potential with normal separation distance) on contact spacing. A nonlinear hydrodynamic stability analysis has been tested here for the first time, against experimental results. Its introduction offers a way of further reconciling the above specific, nonspecific, and permissive concepts in adhesion because it has the potential to accommodate the effects of specific interactions (Florin et al., 1994) that are too short-ranged to influence the linear theory description of the beginning of localized membrane front convergence.

Contact point separation has been examined here over at wider range and a greater number (eight rather than three) of ionic strengths than in earlier work (Thomas and Coakley, 1995). The adhesion experiments on each batch of blood were carried out at all ionic strengths so that variation due to ionic strength rather than to day-to-day variation in blood response was emphasized (Fig. 3).

The -0.25 slope of Fig. 5 gives a fourth root dependence of wavelength on the inverse of the gradient of disjoining pressure. This dependence is consistent with a bending rather than tension-controlled instability (Eq. 8). The intercept of the straight line with the $\log(\lambda)$ axis when $\log(\Delta(d\phi/dh))$ is zero leads to an estimate of 4×10^{-11} dyn·cm for B in Eq. 8. This value is close, considering the length of the extrapolation of the line of Fig. 5 to reach the required intercept, to measured values of 1.8×10^{-12} dyn·cm (Evans, 1983) and 4×10^{-12} dyn/cm (Peterson et al., 1992) for the erythrocyte membrane bending modulus. It was not possible in previous work (Thomas and Coakley, 1995) at three ionic strengths to discriminate between bending and tension control of stability. Acquisition of information at eight ionic strengths in the present work has resulted in data sets that are most reasonably interpreted as supporting a membrane bending rather than tension-controlled mechanism.

The numerical simulations obtained with the nonlinear theory give the following additional insights into the mechanism of local contact formation.

First, the threshold ionic strength for change from parallel contact seams to periodic patterns, which was previously identified in a linear theory, is confirmed here and its significance extended in the nonlinear theory. If the change in ionic strength is considered as a physicochemical constraint imposed on the system, there is a "bifurcation" in the macroscopic state of the system (parallel seam to localized contacts) for ionic strength between 0.065 and 0.075. We can thus follow the new macroscopic state of the system above the threshold, and it can be observed on Fig. 6 that the amplitude of the pattern (distance between the maxima of the SQ mode) will increase with increasing values of ionic strength. The bifurcation is thus supercritical and stable (Erneux and Gallez, 1997).

Second, the emergence of patterns and the trend of change of wavelengths with the ionic strength are in qualitative agreement with the experimental observations (Fig. 6). The nonlinear theory allows the visualization of the symmetric mode (SQ mode) for finite amplitude perturbations, which was impossible with a linear theory that applies only at the onset of the perturbation. The simulations show also that there is an ionic strength dependence of the normal distance of approach between the local contact points (crests of SQ mode). This minimum distance of normal separation decreases as the ionic strength is increased (see Fig. 6 *A*). Because of intermembrane electron microscopy resin it is not possible to measure this separation, so this aspect of the numerical simulation result cannot be confirmed by experimental data. The conclusion can, however, be interpreted in the sense that the order of magnitude of this normal distance

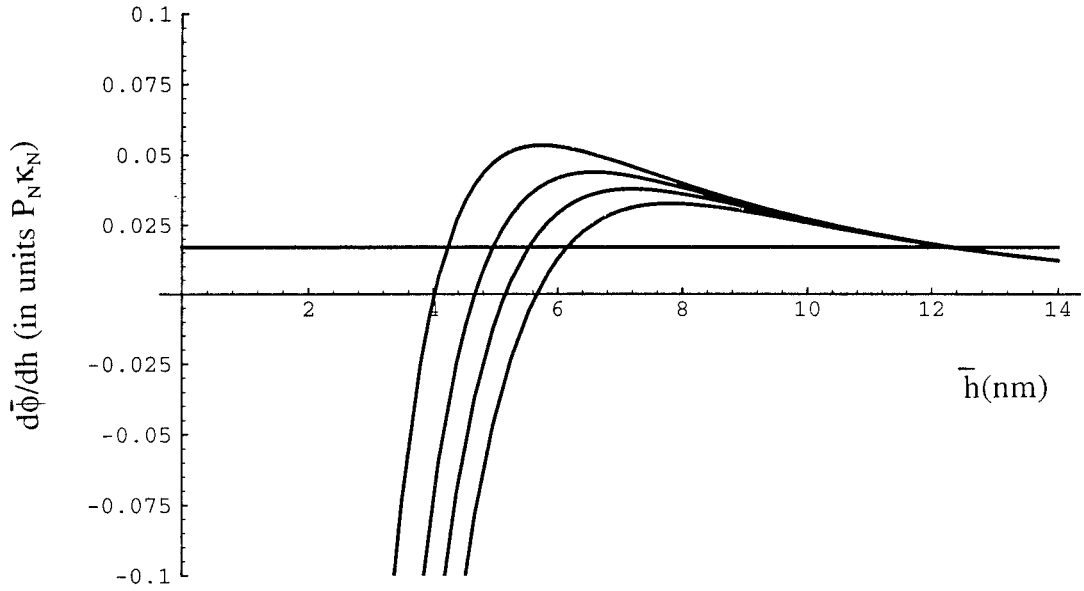

FIGURE 11 Gradient of the disjoining pressure (in units of $P_N\kappa_N$) as a function of the separation distance between the glycocalyxes of two cells (in nm), for 145, 105, 85, and 70 mM [NaCl] *(curves from left to right)*. The horizontal line gives the value of $\bar{B}(2\pi/\bar{\lambda}_m)^4$ in the same units for a dimensional dominant wavelength $\bar{\lambda}_m = 1$ μm. The systems are unstable for the ranges of h values where $d\phi/dh$ exceeds Bq_m^4. The chosen value for the adimensionalization process ($\bar{h}_0 = 12$ nm) is close to the upper limit of the ranges.

is similar to the ionic strength-dependent secondary minimum that would be obtained by conventional equilibrium DLVO theory (Hiemenz, 1986).

Third, the characteristics of the patterns have been tested in different conditions (change of initial conditions, change of the nonelectrical parameters, change of boundary conditions) but the main requirement for stable patterns always remains a balance between repulsive electrical forces and attractive nonelectrical forces. Due to the multiplicity of steady-state solutions in the nonlinear approach, attention has been paid to comparing the results of the different simulations after a sufficiently long time has elapsed.

Fourth, the disjoining pressure concept used in the present theory (linear and nonlinear) can reconcile the choice of different "initial thickness" h_{init} values in interpreting the experimental results of Fig. 5 and the choice of the "average thickness" h_0 to adimensionalize all the quantities for the numerical simulations of the theoretical nonlinear approach. Fig. 11 shows the derivative of the disjoining pressure for different values of the ionic strength. The horizontal line Bq_m^4, which intersects the curves near 12 nm, was used to guide the choice of $\bar{h}_0 = 12$ nm in the adimensionalization procedure. Indeed, following Eq. 7, for systems where tension can be ignored, the system is unstable for the condition

$$Bq_m^4 - d\phi/dh < 0 \qquad (12)$$

This condition is met for the range of $\bar{h}$ values (including $\bar{h}_0 = 12$ nm) for which $d\phi/dh$ exceeds Bq_m^4 (Fig. 11). In view of the discussion of Fig. 5, it is clear that from an experimental point of view any h_{init} satisfying condition (12) is plausible for the formation of patterns.

Fifth, the power of the nonlinear theory could also be extended to describe the dynamics of surface molecules (like receptors) which are able to diffuse along the membrane (Ramos de Souza and Gallez, 1998), in addition to electrostatic effects considered here for tangentially immobile surfaces. Clustering of receptors has already been predicted in a nonlinear analysis, due to the coupling between a chemical reaction and the membrane deformation (Gallez et al., 1996). This confirms the suggestion made previously that cell surface chemistry may affect receptor clustering (Ward and Hammer, 1992). In that sense, extension of the nonlinear theory to the case of specific ligand-receptor interactions involved in bioadhesion processes (Florin et al., 1994) also has significant promise.

Sixth, periodic patterns (termed "blisters") were also observed in adhesion of a giant lipid vesicle, the membrane of which contained charged lipids, to another, supported, membrane (Nardi et al., 1997). Application of the nonlinear interfacial approach to this case shows that blistering and charge separation occur due to mechanical coupling and electrochemical diffusion of the charged lipids (Ramos de Souza et al., submitted for publication).

D.G. acknowledges a grant from the Fonds National de la Recherche Scientifique, Belgium. E.R.S. acknowledges Centro Federal de Educacao Tecnologica da Bahia, Brazil, and the Brazilian Agencies Capes and CNPQ for financial support.

REFERENCES

Acheson, A., J. L. Sunshine, and U. Rutishauser. 1991. NCAM PSA can regulate both cell-cell and cell-substrate interactions. *J. Cell Biol.* 114: 143–153.

Baker, A. J., W. T. Coakley, and D. Gallez. 1993. Influence of polymer concentration and molecular weight and of enzymic glycocalyx modification on erythrocyte interaction in dextran solutions. *Eur. Biophys. J.* 22:53–62.

Bawa, S. R., M. A. Pabst, G. Werner, and H. K. Bains. 1993. Capacitated and acrosome reacted spermatozoa of goat (Capraindicus): a fluorescence and electron microscopic study. *Andrologica.* 25:123–135.

Bennett, V., and D. M. Gilligan. 1993.The spectrin-based membrane skeleton and micron-scale organization of the plasma membrane. *Annu. Rev. Cell Biol.* 9:27–66.

Burridge, K., and M. Chrzanowska-Wodnicka. 1996. Focal adhesins, contractility, and signalling. *Annu. Rev. Cell Dev. Biol.* 12:463–519.

Capo, C., P. Bongrand, A. M. Benoliel, A. Ryter, and R. Depieds. 1981 Particle-macrophage interaction: role of surface charges. *Annales d'Immunol. Institut Pasteur.* 132D:165–173.

Chien, S., S. Simchon, R. E. Abbott, and K.-M. Jan. 1977. Surface adsorption of dextrans on human red blood cell membranes. *J. Colloid Interface Sci.* 62:461–470.

Darmani, H., and W. T. Coakley. 1990. Membrane-membrane interactions: parallel membranes or patterned discrete contacts. *Biochim. Biophys. Acta.* 1021:182–190.

Darmani, H., and W. T. Coakley. 1991. Contact patterns in concanavalin A agglutinated erythrocytes. *Cell Biophys.* 18:1–13.

De Wit, A., D. Gallez, and I. Christov. 1994. Nonlinear evolution equations for thin liquid films with insoluble surfactants. *Phys. Fluids.* 6:3256–3266.

Dimitrov, D. S., and R. K. Jain. 1984. Membrane stability. *Biochim. Biophys. Acta.* 779:437–468.

Donath, E., L. Pratsch, H.-J. Baumler, A. Voigt, and M. Teager. 1989. Macromolecule depletion at membranes. *Stud. Biophys.* 130:117–122.

Donath, E., and A. Voigt. 1983. Charge distribution within cell surface coats of single and interacting surfaces: a minimum free electrostatic energy approach. Conclusions for electrophoretic mobility measurements. *J. Theor. Biol.* 101:569–584.

Erneux, T., and D. Gallez. 1997. Can repulsive forces lead to stable patterns in thin liquid films? *Phys. Fluids.* 9:1194–1196.

Evans, E. 1995. Physical actions in biological adhesion, *In* Handbook of Biological Physics, Vol. 1. R. Lipowsky and E. Sackmann Eds., Elsevier, Amsterdam.

Evans, E. A. 1983. Bending elastic modulus of red cell membranes derived from buckling instability in micropipette aspiration experiments. *Biophys. J.* 43:27–30.

Evans, E. A. 1989. Force between surfaces that confine a polymer solution: derivation from self-consistent field theories. *Macromolecules.* 22: 2277–2286.

Evans, E., and D. Needham. 1988. Attraction between lipid bilayer membranes in concentrated solutions of nonadsorbing polymers: comparison of mean-field theory with measurements of adhesion energy. *Macromolecules.* 21:1822–1831.

Fisher, L. 1993. Forces between biological surfaces. *Chem. Soc. Faraday Trans.* 89:2567–2582.

Florin, E. L., V. T. Moy, and H. E. Gaub. 1994. Adhesion forces between individual ligand/receptors pairs. *Science.* 264:415–417.

Flyer, H. J. L., and S. Hockfield. 1996. The role of polysialic acid and other carbohydrate polymers in neural structural plasticity. *Curr. Opin. Neurobiol.* 6:113–118.

Foa, C., M. Soler, A.-M. Benoliel, and P. Bongrand. 1996. Steric stabilization and cell adhesion. *J. Mater. Sci.: Mater. Med.* 7:141–148.

Gallez, D., and W. T. Coakley. 1986. Interfacial instability at cell membranes. *Prog. Biophys. Mol. Biol.* 48:155–199.

Gallez, D., and W. T. Coakley. 1996. Far-from-equilibrium phenomena in bioadhesion processes. *Heter. Chem. Rev.* 3:443–475.

Gallez, D., A. De Wit, and M. Kaufman. 1996. Dynamics of a thin liquid film with a surface chemical reaction. *J. Colloid Interface Sci.* 180: 524–536.

Hiemenz, P. C. 1986. Principles of Colloid and Surface Chemistry. Marcel Dekker, New York.

Hoffman, J. F., and P. C. Laris. 1974. Determination of membrane potentials in human and amphiuma red blood cells by means of a fluorescent probe. *J. Physiol. (Lond.).* 239:519–552.

Jan, K.-M. 1979. Role of hydrogen bonding in cell aggregation. *J. Cell Physiol.* 101:49–55.

Khanna, R., and A. Sharma. 1997. Pattern formation in spontaneous dewetting of thin apolar films. *J. Colloid Interface Sci.* 195:42–50.

Levine, S., M. Levine, K. A. Sharp, and D. E. Brooks. 1983. Theory of the electrokinetic behavior of human erythrocytes. *Biophys. J.* 42:127–135.

McIver, D. J. L., and S. Church. 1982. Interfacial free energies of intact and reconstituted erythrocyte surfaces: implication for biological adhesion. *Biochim. Biophys. Acta.* 691:52–60.

Mitlin, V. S. 1993. Dewetting of solid surfaces: analogy with spinodal decomposition. *J. Colloid Interface Sci.* 156:491–497.

Nardi, J., T. Feder, R. Bruinsma, and E. Sackmann. 1997. Electrostatic adhesion between fluid membranes: phase separation and blistering. *Europhys. Lett.* 37:371–376.

Peterson, M. A., H. Strey, and E. Sackmann. 1992. Theoretical and phase contrast microscopic eigenmode analysis of erythrocyte flicker amplitudes. *J. Phys. II (France).* 2:1273–1285.

Press, W. H., B. P. Flannery, S. A. Teukolsky, and W. T. Vetterling. 1989. Numerical Recipes. Cambridge University Press, Cambridge.

Prevost, M., and D. Gallez. 1986. Nonlinear disruption of thin free liquid films. *J. Chem. Phys.* 84:4043–4048.

Rabinovitch, M. 1971. Phagocytosis of erythrocytes by *Acanthamoeba* species. *Exp. Cell Res.* 64:275–284.

Ramos de Souza, E., and D. Gallez. 1998. Pattern formation in thin liquid films with insoluble surfactants. *Phys. Fluids.* 10:1804–1814.

Rutishauser, U. 1996. Polysialic acid and the regulation of cell interactions. *Curr. Opin. Cell Biol.* 8:679–684.

Rutishauser, U., and L. Landmesser. 1996. Polysialic acid in the vertebrate nervous system: a promoter of plasticity in cell-cell interactions. *TINS.* 19:422–427.

Saghir, N. 1997. Phagocytosis and cell surface properties. Ph.D. thesis, University of Wales.

Snowden, M. J., S. M. Clegg, and P. A. Williams. 1991. Flocculation of silica particles by adsorbing and non-adsorbing polymers. *J. Chem. Soc. Faraday Trans.* 87:2201–2207.

Sung, L. A., and E. A. Kabat. 1994. Agglutination-induced erythrocyte deformation by two blood group A-specific lectins: studies by light and electron microscopy. *Biorheology.* 31:353–364.

Thomas, N. E., and W. T. Coakley. 1995. Localized contact formation by erythrocyte membranes: electrostatic effects. *Biophys. J.* 69:1387–1401.

Viitala, J., and J. Jarnefelt. 1985. The red cell surface revisited. *Trends Biochem. Sci.* 10:392–395.

Ward, M. D., and D. A. Hammer. 1992. Morphology of cell-substratum adhesion. *Cell Biophys.* 20:177–222.

Ward, M. D., and D. A. Hammer. 1993. A theoretical analysis for the effect of focal contact formation on cell-substrate attachment strength. *Biophys. J.* 64:936–959.

Weiss, L., E. Mayhew, and K. Ulrich. 1966. The effect of neuraminidase on the phagocytic process in human monocytes. *Lab. Invest.* 15: 1304–1309.

Yang, P., D. Major, and U. Rutishauser. 1994. Role of charge and hydration in effects of PSA on molecular interactions on and between membranes. *J. Biol. Chem.* 269:23039–23044.